

# Photoinduced Hund excitons in the breakdown of a two-orbital Mott insulator

Julián Rincón,<sup>1</sup> Elbio Dagotto,<sup>2,3</sup> and Adrian E. Feiguin<sup>4</sup>

<sup>1</sup>*Perimeter Institute for Theoretical Physics, Waterloo, Ontario N2L 2Y5, Canada*

<sup>2</sup>*Department of Physics and Astronomy, The University of Tennessee, Knoxville, Tennessee 37996, USA*

<sup>3</sup>*Materials Science and Technology Division, Oak Ridge National Laboratory, Oak Ridge, Tennessee 37831, USA*

<sup>4</sup>*Department of Physics, Northeastern University, Boston, Massachusetts 02115, USA*

(Dated: July 3, 2017)

We study the photoinduced breakdown of a two-orbital Mott insulator and resulting metallic state. Using time-dependent density matrix renormalization group, we scrutinize the real-time dynamics of the half-filled two-orbital Hubbard model interacting with a resonant radiation field pulse. The breakdown, caused by production of doublon-holon pairs, is enhanced by Hund's exchange, which dynamically activates large orbital fluctuations. The melting of the Mott insulator is accompanied by a high- to low-spin transition with a concomitant reduction of antiferromagnetic spin fluctuations. Most notably, the overall time response is driven by the photogeneration of excitons with orbital character that are stabilized by Hund's coupling. Such Hund excitons, which can form a condensate, correspond to bound doublon-holon pairs with spin-singlet and orbital-triplet quantum numbers. Hund excitons are not directly bound by Coulomb or Hubbard- $V$  interactions, as other excitons, but due to Hund's exchange. We study exciton properties such as bandwidth, binding potential, and size within a semiclassical approach. The photometallic state, which results from a coexistence of Hund excitons and doublon-holon plasma, differs with the equilibrium concept of Hund's metal used in multiorbital physics.

## I. INTRODUCTION

Control over the electronic properties of quantum matter using electromagnetic radiation is an attainable route to efficiently and systematically understand nonequilibrium phenomena. The interaction of correlated matter with light fields has already uncovered a wealth of exotic "hidden" phases [1, 2] including light-induced superconductivity [3], dielectric breakdown in solids [4–7], photometallic states in organic insulators [8], and photodisruption of charge, magnetic, and orbital order in complex oxides [9–12].

For the photoinduced dielectric breakdown in insulators, the optical excitations typically observed are holons, doublons, and excitons. Excitons are neutral highly polarizable bound states, resulting from attractive Coulomb interactions, formed by particle-hole pairs. In the case of Mott insulators the particle-hole pair is made out of a holon and a doublon (doubly occupied state). Excitons are classified depending on the strength of Coulomb interactions and the dielectric properties of the medium in which they propagate [13, 14]. *Wannier-Mott* excitons are realized when the particle-hole interaction is weak, giving rise to an exciton with a large radius (defined by the particle-hole separation). These excitons are typically found in semiconductors. *Frenkel* excitons, on the other hand, are tightly bound with a small particle-hole radius. Conjugated polymers and molecular crystals usually display this type of excitons. *Mott-Hubbard* excitons are bound states that usually arise from local Coulomb interactions such as Hubbard- $V$  terms. Excitons of this sort have been proposed to explain optical properties in quantum materials such as complex oxides.

Partial or complete melting of insulating behavior with strong ultrashort light pulses has been experimentally ex-

plored measuring reflectivity and absorptivity. Indeed ultrafast photodoping in the one-dimensional Mott insulator ET-F<sub>2</sub> TCNQ has induced a metastable metallic behavior, where electron interactions still play a dominant role in the recombination dynamics of the carriers: doublon-holon pairs [5]. By applying pressure to the same material it is possible to tune the electronic structure and interactions, controlling the generation of Mott-Hubbard excitons and controlling their recombination dynamics [15]. Similarly, reversible control over the charge gap in fused silica has been achieved with strong few-cycle fields without damaging the sample. The dielectric breakdown signaled by the charge gap melting leads to a concomitant current increase of over 18 orders of magnitude within 1 femtosecond, implying a highly nontrivial photocarrier dynamics [6, 7].

Photoinduced states in insulator complex-oxides, where orbital degrees of freedom play a relevant role, have also been studied. An insulator-metal phase transition generated with light in the manganite Pr<sub>0.7</sub>Ca<sub>0.3</sub>MnO<sub>3</sub> was reported [9]. Using optical reflectivity measurements it was shown the emergence of a metallic phase, and corresponding melting of charge and orbital order, along with coherent orbital oscillations. This state is not present in the phase diagram of such compound. Analogously, a photoinduced phase transition to a long-lived ferromagnetic metallic state was observed in the strained insulating manganite La<sub>2/3</sub>Ca<sub>1/3</sub>MnO<sub>3</sub>, where the cooperative formation of spin oriented conducting paths was suggested as the main mechanism leading to the hidden metallic state [11].

A considerable theoretical effort has been devoted to understanding the photoinduced insulator-metal transition [16–27]. Dielectric breakdown of single-orbital Mott insulators, modeled with the Hubbard model, has been

studied using variational methods [16–20] and dynamical mean field theory [21, 22]. The key findings in these efforts is that after interaction with a field pulse the Mott insulating state transitions to a quasi-stationary bad metallic state with finite current. The metallic state survives due to Landau-Zener quantum tunneling between many-body states. Additionally, the breakdown depends not only on the field strength but also on the electron interactions (Hubbard- $U$ ). Light-induced phenomena in two-orbital models has been studied focusing mainly in quarter-filled Mott insulators using double-exchange models [23–27]. A field-generated phase transition from an insulating state to a ferromagnet was observed, along with a related low- to high-spin transition. The low-spin state is formed by bound states of high-spin states and holes. Orbital coherent oscillations in the photoresponse of the Mott insulating state have also been reported [24].

Here, using the density matrix renormalization group (DMRG) [28, 29], we study the breakdown of a Mott insulator state in the half-filled two-orbital Hubbard model. In this work we show that the carrier dynamics generated by photoirradiation uncover a new type of exciton. Such exciton is different from those discussed previously in the sense that it is not directly realized due to Coulomb but to exchange interactions; more precisely, Hund’s coupling. We study the overall effect of Hund’s exchange on the photodynamics and corresponding dielectric breakdown of the Mott insulator. This is accomplished by using time-dependent DMRG [30–32] and calculating a variety of observables. The presence of light, which is treated classically, is taken into account via a Peierls substitution in the hopping. We have considered light pulses with few cycles due to their experimental relevance. The main findings in this work can be summarized as follows.

First, Hund’s exchange enhances the breakdown of the Mott insulator (understood as a light-induced production of doublons) with the concomitant partial melting of antiferromagnetic (AFM) fluctuations and associated high- to low-spin and insulator-metal photoinduced phase transitions. The resulting long-lived state is a photoinduced metallic state.

Second, it is known that Hund’s rule coupling acts as an orbital decoupler at equilibrium, locking orbital fluctuations and yielding orbital differentiation phenomena. Here, however, it acts as a *dynamical coupling* for the field-induced dynamics activating large orbital fluctuations.

Third, we observe the emergence of neutral bound optical excitations with low spin and orbital character. The coherence of these “Hund excitons” leads to the photoinduced metallic state. This type of optical excitation is associated to the presence of Hund’s exchange, challenging the belief that only direct Coulomb interaction leads to exciton formation.

The rest of the paper is organized as follows. In Sec. II we introduce the two-orbital Hubbard Hamiltonian and its ground state properties, the numerical procedure fol-

lowed, and the observables calculated. Section III is devoted to the analysis of the photodynamics. We finally close in Sec. IV with the conclusions of our effort.

## II. THEORETICAL CONSIDERATIONS

In this section we describe the model Hamiltonian, corresponding parameters used in our study, and the observables calculated to analyzed the photodynamics in a two-orbital Mott insulator. We also discuss some basic properties of the half-filled Mott insulating state.

### A. Model Hamiltonian

We explore a two-orbital Hubbard model Hamiltonian which includes kinetic energy, intra- and inter-orbital local Coulomb repulsion, Hund’s rule exchange coupling, and pair-hopping process. Explicitly,

$$\begin{aligned}
 H = & - \sum_{i\sigma\gamma} t_\gamma \left( c_{i\sigma\gamma}^\dagger c_{i+1\sigma\gamma} + \text{H.c.} \right) + U \sum_{i\gamma} n_{i\uparrow\gamma} n_{i\downarrow\gamma} \\
 & - 2J \sum_i \mathbf{S}_{i1} \cdot \mathbf{S}_{i2} + (U' - J/2) \sum_i n_{i1} n_{i2} \quad (1) \\
 & + J \sum_i \left( c_{i\uparrow 0}^\dagger c_{i\downarrow 0}^\dagger c_{i\downarrow 1} c_{i\uparrow 1} + \text{H.c.} \right),
 \end{aligned}$$

where we consider a one-dimensional geometry of  $N$  sites, or equivalently  $2N$  orbitals, whose sites are labeled by  $i$ . The operator  $c_{i\sigma\gamma}$  ( $c_{i\sigma\gamma}^\dagger$ ) annihilates (creates) a particle at site  $i$ , spin projection  $\sigma$  at orbital  $\gamma = 1, 2$ . The density  $n_{i\sigma\gamma}$  and spin  $\mathbf{S}_{i\gamma}$  operators are written in the standard form in terms of  $c_{i\sigma\gamma}$  and  $c_{i\sigma\gamma}^\dagger$ . The hopping parameters  $t_\gamma$  are orbital-dependent.  $U$  and  $J$  stand for Hubbard repulsion and Hund’s ferromagnetic exchange, and  $U' = U - 2J$  is used for symmetry reasons.

### B. Light pulse

To account for the interaction with a light pulse we employ the so-called Peierls substitution, where the *classical* light field enters in the Hamiltonian through the kinetic energy operator. We therefore introduce a time  $\tau$  dependence in the hopping integrals

$$t_\gamma \longrightarrow t_\gamma(\tau) = t_\gamma \exp(iA(\tau)/N), \quad (2)$$

where  $N$  stands for the system size. The time-dependent phase is actually the vector potential of light whose form is assumed to be an oscillatory Gaussian pulse

$$A(\tau) = A_0 \exp \left[ -\frac{(\tau - \tau_P)^2}{2\sigma_P^2} \right] \cos [\omega_P(\tau - \tau_P)]. \quad (3)$$

The frequency  $\omega_P$ , intensity  $A_0$ , width  $\sigma_P$ , and peak time  $\tau_P$  characterize the nature of the electric field of the light

pulse, for which we neglect its dynamics and assumed to be a classical field. In the calculations presented here we have only considered few-cycle pulses given its experimental relevance.

### C. Parameters and procedure

The procedure followed for the calculation of the time dependent properties of the two-orbital Hubbard model is as follows. We first calculate the ground state of Hamiltonian (1), without light field ( $A(\tau) = 0$ ), using ground-state DMRG [28, 29]. Once the energy has been minimized and the wavefunction  $|\Psi_0\rangle$  is accurately represented, we switch on the vector potential and perform a real-time evolution of the ground state using the now time-dependent Hamiltonian (1) and solving for the wavefunction through the equation  $|\Psi(\tau+d\tau)\rangle = \exp(-i \int_{\tau}^{\tau+d\tau} d\tau' H(\tau')) |\Psi(\tau')\rangle$ , with initial condition  $|\Psi(\tau=0)\rangle = |\Psi_0\rangle$ . The time evolution is performed using time-dependent DMRG with a fourth-order Runge-Kutta integrator to adapt the basis [29, 32, 33], with a Krylov expansion of the evolution operator [33]. With  $|\Psi(\tau)\rangle$  for different time slices we can calculate expectation values and watch their time evolution. The DMRG simulations were performed for systems from 8 up to 32 orbital sites with a discarded weight of less than  $10^{-8}$ . We note that the finite-size effect in this model has been shown to be quite small. Typically, for  $N \gtrsim 8$  such effects are negligible for the purpose of our investigations.

The parameters of the Hamiltonian to be used are  $t_\gamma = (-0.5, -0.5)$  and  $U = 8$ , with a filling factor of one particle per orbital, i.e. half-filling, and we will explore results for the ratios  $J/U = 0, 0.1, 0.25$ . We have chosen a diagonal hopping matrix merely for simplicity, based on previous work [34, 35]. Materials such as the iron-based superconductors have  $J/U$  as large as  $1/4$  [36]. The bandwidth for each orbital is  $W_\gamma = 4t_\gamma$ . We will refer to the case when  $W_1 = W_2$  as *isotropic*. The name is related to the presence of a  $U(1)_o$  symmetry associated to the orbital channel. For the isotropic case the full symmetry of the system is  $U(1)_c \times SU(2)_s \times U(1)_o$ , where the subindices refer to charge conservation ( $c$ ), spin rotational symmetry ( $s$ ), and orbital rotational symmetry ( $o$ ). The parameters used for the light field are  $A_0 = 2.4$ ,  $\sigma_P = 0.19$ ,  $\tau_P = 4\sigma_P$ , finally,  $\omega_P = \Delta$  the frequency of the pulse was set to match the charge gap  $\Delta$  of the Mott insulator ground state.

### D. Observables

In order to study the time response of the system we explore the following observables. The total double occupancy is

$$D_{\text{tot}}(\tau) = \frac{1}{N} \sum_i \langle \Psi(\tau) | n_{i\uparrow} n_{i\downarrow} | \Psi(\tau) \rangle. \quad (4)$$

The local magnetic moment is

$$\langle S^z(\tau)^2 \rangle = \frac{1}{N} \sum_i \langle \Psi(\tau) | (S_i^z)^2 | \Psi(\tau) \rangle. \quad (5)$$

The orbital-dependent static spin structure factor is

$$S_\gamma(q, \tau) = \frac{1}{N} \sum_{jk} e^{iq(j-k)} \langle \Psi(\tau) | S_{j\gamma}^+ S_{k\gamma}^- | \Psi(\tau) \rangle. \quad (6)$$

Inter-orbital local charge fluctuations are

$$C_{12}(\tau) = \frac{1}{N} \sum_i \langle \Psi(\tau) | \delta n_{i1} \delta n_{i2} | \Psi(\tau) \rangle, \quad (7)$$

where  $\delta n_{i\gamma} := n_{i\gamma} - \langle \Psi(\tau) | n_{i\gamma} | \Psi(\tau) \rangle$ . The local holon  $[n_{i\gamma}^h := (1 - n_{i\uparrow\gamma})(1 - n_{i\downarrow\gamma})]$  doublon  $(n_{i\gamma}^d := n_{i\uparrow\gamma} n_{i\downarrow\gamma})$  number correlation function is defined as

$$C_{\text{loc}}^{dh}(\tau) = \frac{1}{N} \sum_i \langle \Psi(\tau) | n_{i1}^d n_{i2}^h + n_{i1}^h n_{i2}^d | \Psi(\tau) \rangle. \quad (8)$$

Similarly the orbital nearest-neighbor doublon-holon correlation function is

$$C_\gamma^{dh}(\tau) = \frac{1}{N-1} \sum_i \langle \Psi(\tau) | n_{i\gamma}^d n_{i+1\gamma}^h + n_{i\gamma}^h n_{i+1\gamma}^d | \Psi(\tau) \rangle. \quad (9)$$

In the plots shown in this paper the ordinate axis actually represents the relative change of any of the abovementioned expectation values with respect to their ground state value. That is, any expectation value  $\mathcal{E}_a(\tau)$ , which depends on time and have quantum numbers packed as a single index  $a$ , will be plotted as

$$\Delta \mathcal{E}_a(\tau) := \frac{\mathcal{E}_a(\tau) - \mathcal{E}_a(\tau=0)}{\mathcal{E}_a(\tau=0)}. \quad (10)$$

For simplicity we will label the ordinate axis by  $\mathcal{E}_a(\tau)$  instead of  $\Delta \mathcal{E}_a(\tau)$ . For instance, for the total double occupancy we will plot

$$\Delta D_{\text{tot}}(\tau) := \frac{D_{\text{tot}}(\tau) - D_{\text{tot}}(0)}{D_{\text{tot}}(0)}, \quad (11)$$

but label the ordinate axis in the plots as just  $D_{\text{tot}}(\tau)$ . An important exception will be the expectation value of the current density operator defined as

$$J(\tau) = \frac{i}{N-1} \sum_{j\sigma\gamma} t_\gamma \langle \Psi(\tau) | c_{j\sigma\gamma}^\dagger c_{j+1\sigma\gamma} - \text{H.c.} | \Psi(\tau) \rangle, \quad (12)$$

for  $\tau > 2\tau_P$ , for which we will just simply plot as  $J(\tau)$ .

### E. On the nature of the ground state

Let us first discuss the nature of the ground state of the two-orbital Hubbard model at half-filling. Regardless of the values of  $U/W_\gamma$ , the system has a finite single-particle gap, signaling an insulating state. In the absence

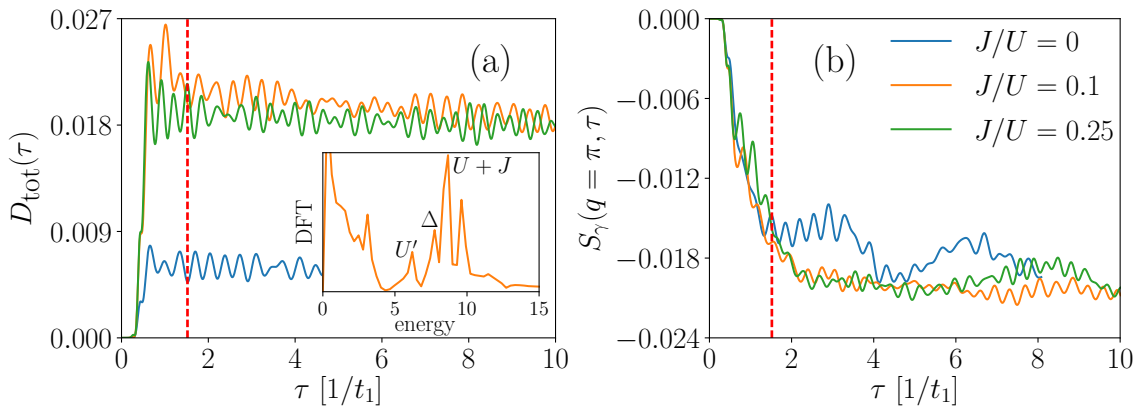


FIG. 1. Total double occupancy (a) and antiferromagnetic fluctuations (b), peak at  $q = \pi$ , for several values of  $J/U$  and  $U = 8$ . The vertical dashed line marks the light pulse span. (a) Breakdown of the Mott insulating state is signaled by the creation of doublons. Inset: discrete Fourier transform (DFT) of  $D_{\text{tot}}(\tau)$ , for  $J/U = 0.1$  (color coded with main figure), showing the characteristic energy scales associated to the oscillations in the time response. (b) In parallel, although within a different timescale, the AFM order is partially melted.

of Hund's coupling, the ground state is weakly magnetic with no large AFM and large orbital fluctuations. For finite values of  $J$ , the ground state has a local magnetic moment leading to the establishment of quasi-long-range antiferromagnetic correlations with a large suppression of fluctuations in the orbital channel. The imbalance in the bandwidths of the orbitals will still favor antiferromagnetic order and, under the appropriate conditions, the orbital differentiation phenomena [37].

### III. RESULTS FOR THE PHOTODYNAMICS

The results for the photodynamics in the isotropic case are shown in Figs. 1-3. We start by pointing out that the time response in different orbitals is the same due to the degeneracy in orbital space and hence we only plot results for one orbital. Let us explore the case  $J = 0$  first. As discussed above the ground state in this case is paramagnetic, which implies that the doublon number is large (at least compared to the case  $J \neq 0$ ). The large amount of doublons in the ground state has to do with small magnetic and large orbital fluctuations; therefore, the resulting light-induced doublon production is weak. As shown in Fig. 1 (a), the effective photodoping in this case (measured as the amount of doublon or holons generated with respect to the ground state) is about 0.6%. The period of the oscillations are  $2\pi/U$  and  $2\pi/\Delta$ , where  $\Delta$  corresponds to the single-particle gap, see inset plot for details.

In contrast, the case of finite  $J$  leads to a larger production of doublon-holon pairs and hence to a stronger breakdown of the insulating state, see Fig. 1 (a). (The breakdown of the insulator is to be understood here as the production of doublon-holon pairs, which constitute the carriers.) We observe that for fairly large values of  $J/U$  the photodoping rate lies around 20%. We can then say that Hund's exchange enhances the melting of the

Mott insulator. Notice that a finite  $J$  lifts the degeneracy of the atomic states giving rise to the following periods of oscillation:  $2\pi/U'$ ,  $2\pi/\Delta$ , and  $2\pi/(U + J)$ . We see that the effective local Coulomb repulsion has been renormalized by  $J$ . As it will be discussed later, the latter period is associated to the photogeneration of spin-singlet orbital-triplet doublons.

The doublon-holon pair production leads to a concomitant partial melting of the magnetic order, at least for  $J \neq 0$ . We plot in Fig. 1 (b) the value of the spin structure factor at the ordering wave vector  $q/\pi = 1$ . We observe a cooperative phenomenon where the melting of the AFM order happens simultaneously as doublons are produced. The typical time scale at which  $S(q = \pi, \tau)$  decays is related to the single-particle charge gap  $\Delta$ , which in the atomic limit goes as  $\Delta^{\text{at}} \sim U + J$  such that the decrease in the AFM fluctuations happens at larger time scales for finite  $J$ .

The light-induced production of carriers can be associated with a reduction in the local magnetic moment. The time evolution of  $\langle S^z(\tau)^2 \rangle$ , as shown in Fig. 2 (a) for several values of  $J/U$ , indicates a decrease in the local magnetic moment when interacting with light. Such a change is in agreement with both doublon production and melting of magnetic order and signals a high- to low-spin photoinduced phase transition. Similarly to the case of  $S(q = \pi, \tau)$  the reduction in the magnetic moment is only partial and so is the phase transition between local spin states, where  $\langle S^z(\tau)^2 \rangle$  has been reduced by up to 1%.

In order to examine the photodynamics in the orbital channel we show in Fig. 2 (b) the change in the orbital fluctuations,  $C_{12}(\tau)$ , as a function of time  $\tau$ . We observe this change to be negligible for  $J = 0$ . The situation completely changes when  $J/U \neq 0$ , where large variations in  $C_{12}$  are detected. We also notice that larger values of  $J/U$  lead to larger fluctuations. The negative deviations for  $J/U = 1/4$  show that orbital fluctuations

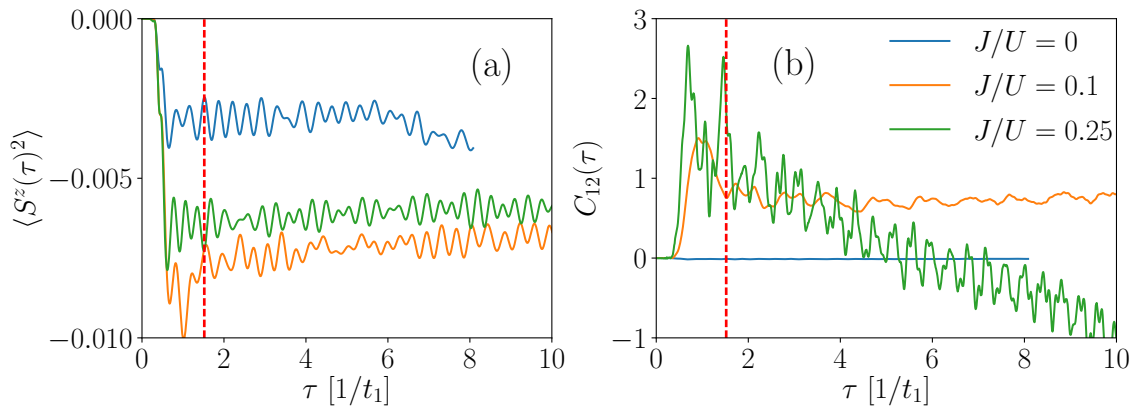


FIG. 2. Local magnetic moment (a) and inter-orbital local charge fluctuations (b) for several values of  $J/U$ . The vertical dashed line marks the light pulse span. (a) A decrease in the local magnetic moment is indicative of a high- to low-spin transition induced by the field. (b) The dynamical coupling effect of Hund's exchange can be seen in the inter-orbital charge fluctuations.

tuations at long times decrease compared to the ground state value, still indicating a substantial change in orbital correlations. The light-induced activation of correlations in the orbital channel, as seen in the time dependence of  $C_{12}(\tau)$ , reaches an order-of-magnitude increase when compared to the ground state case. At equilibrium, Hund's coupling tends to lock orbital correlations leading to the formation of robust magnetic moments and order; whereas in the nonequilibrium case, Hund's exchange *dynamically* favors orbital excitations and melting of such magnetic moments. The activation of orbital fluctuations is due to the suppression of the magnetic order and corresponding generation of doublons which can hop through the system via second-order- and pair-hopping processes. This makes the coupling of orbitals stronger than in the ground state scenario.

The partial melting of the AFM order, the concomitant high- to low-spin photoinduced transition, and the large orbital fluctuations (with the corresponding oscillation frequency  $U + J$  associated to spin-singlet orbital-triplet doublons) indicate that the doublons and holons arrange in an unexpected way in the photodynamics. We confirm this expectation by studying the inter-orbital local and intra-orbital neighboring correlations between holon and doublon number operators,  $C_{\text{loc}}^{\text{dh}}$  and  $C_{\gamma}^{\text{dh}}$  respectively. The results are shown in Fig. 3 (a) and (b), respectively. We observe that similarly to  $C_{12}(\tau)$  the local doublon-holon number correlation function displays robust changes, as large as 60% up to 150%, compared to the ground state [see Fig. 3 (a)]. On the other hand, the neighboring intra-orbital doublon-holon number correlation presents smaller changes, of around 10 – 20%, compared to  $C_{\text{loc}}^{\text{dh}}$  [shown in Fig. 3 (b)]. We can clearly see the effect of Hund's rule coupling in the photoinduced dynamics: without  $J$  there is no appreciable change in both  $C_{\text{loc}}^{\text{dh}}$  and  $C_{\gamma}^{\text{dh}}$ , and large values of  $J/U$  leads to a larger response in these observables. As discussed above, the larger effect in  $C_{\text{loc}}^{\text{dh}}(\tau)$  is associated to pair- and second-order-hopping processes along with spin fluctu-

ations, which do not necessarily enhance  $C_{\gamma}^{\text{dh}}(\tau)$ .

### Exciton properties

We interpret the abovementioned results as the *photogeneration of neutral low-spin objects with orbital character that are bound locally*, suggesting they are novel excitons. More specifically, the photodynamics generates spin-singlet orbital-triplet doublon-holon bound pairs induced by  $J$ . These excitations move in an AFM background with an effective bandwidth of around

$$W_{\text{excitons}} \sim \frac{t_1 t_2}{U - 3J}. \quad (13)$$

Naively it is expected that the excitons, which are naturally Bosons, will propagate coherently giving rise to a condensate, in the low-density limit. In the Fermionic language we obtain a metallic state, as confirmed by the electric current shown in Fig. 6. As noted above, these excitons are created due to the presence of Hund's rule exchange coupling; therefore their existence is *not* directly related to Coulomb interactions. These findings suggest that the type of excitons observed here correspond to a kind of optical excitation that is set apart from more familiar quasiparticles, such as Frenkel, Mott-Hubbard, and Wannier-Mott excitons, which are typically associated to large or small Coulomb interactions. A cartoon showing the photogeneration of such excitons and their emergent dynamics is shown in Fig. 4, see caption for details.

The stability of the excitons can be understood by considering the two-orbital AFM insulating state in the Ising limit (ignoring spin fluctuations) and assuming the creation of a single doublon-holon pair locally, as shown in Fig. 5. For illustration, one can allow the doublon to move through hopping processes, creating a string of misaligned spins in the AFM background, separating it from the holon (see Fig. 5). This will induce a linear confining

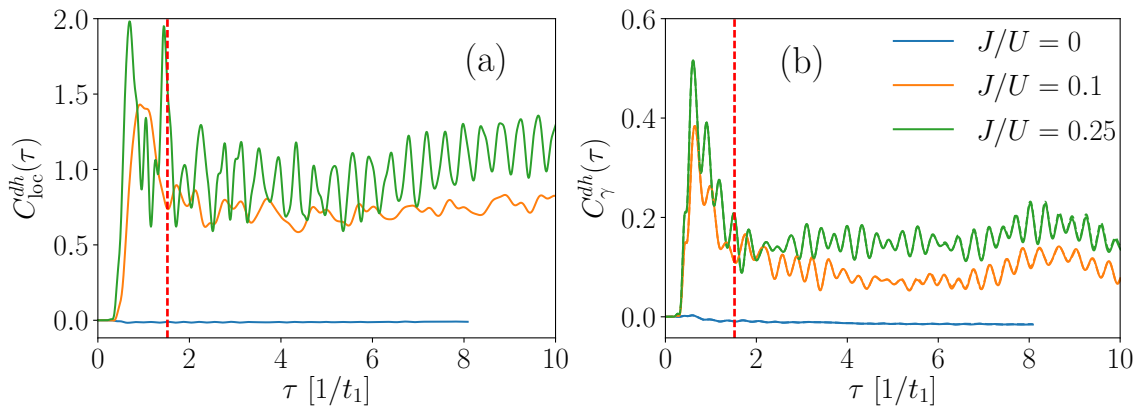


FIG. 3. Local (a) and neighboring (b) doublon-holon correlation function for several values of  $J/U$ . The vertical dashed line marks the light pulse span. Large fluctuations in the local doublon-holon number correlation (a), when compared to the neighboring one (b), suggest that doublon and holon will tend to bound on the same site and different orbitals rather than within neighboring sites in the same orbital.

potential  $V_{\text{excitons}}(x)$ , at position  $x$ , that will favor the motion of both holon and doublon as a single “heavier” object, with the bandwidth (13). The confining potential reads

$$V_{\text{excitons}}(x = ja) \sim J|x|, \quad (14)$$

where  $J$  corresponds to Hund’s coupling,  $j$  labels a site, and  $a$  is the lattice spacing. In order to arrive to this result we have only considered the Hund exchange in the

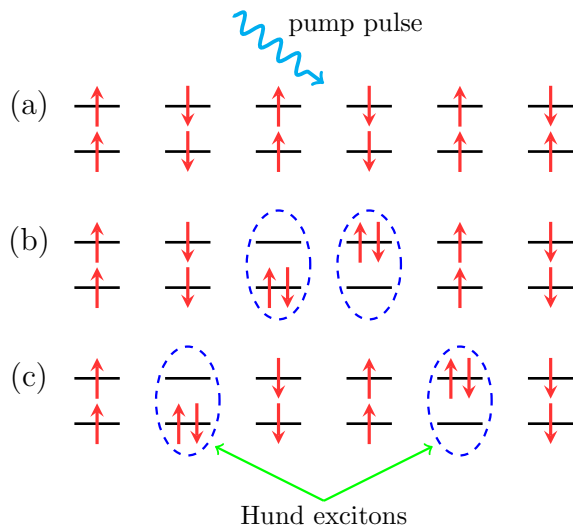


FIG. 4. Cartoon of the dynamical formation of excitons in a one-dimensional two-orbital Mott insulator. (a) The starting point is the Mott insulator ground state interacting with the incident light. (b) After photo-irradiation doublon-holon pairs are created by absorption of photons, which bound to form excitons (dashed ellipses). (c) Such excitons will move in the lattice with a characteristic bandwidth (13) and size (17). While in principle there are other possible states that can be generated from panel (a) after the absorption of a photon, our results indicate that panel (b) is the most likely.

$z$  direction. Notice that existence of the confining potential is directly linked to a finite value of Hund’s rule coupling. If  $J = 0$  there is no confining potential allowing the doublons and holons to move independently.

We can also estimate the size of the exciton by writing down an effective model for the motion of a doublon (or a holon) in the presence of the exciton potential (14). The effective Hamiltonian is  $H_{\text{eff}} = -\sum_m t_0|m\rangle\langle m+1| + t_0|m+1\rangle\langle m| - V_{\text{excitons}}(m)|m\rangle\langle m|$ , where  $t_0 = \max(t_1, t_2)$  and  $|m\rangle$  corresponds to a Wannier orbital at lattice site  $m$ . Writing down the wave function of the doublon as  $|\text{doublon}\rangle = \sum_m c_m|m\rangle$  we obtain the following time-independent Schrödinger equation

$$E c_m = -t_0(c_{m-1} + c_{m+1}) + V_{\text{excitons}}(m)c_m, \quad (15)$$

where  $E$  stands for the energy. By taking the continuum limit of this equation one obtains

$$-t_0 \frac{d^2 c_x}{dx^2} + V_{\text{excitons}}(x)c_x = E c_x. \quad (16)$$

By re-expressing it in terms of dimensionless variables, one obtains the size of the excitons as the characteristic length scale of the problem:

$$\ell_{\text{excitons}} \sim a \left( \frac{t_0}{J} \right)^{1/3}. \quad (17)$$

For the set of parameters considered in this work we find that  $\ell_{\text{excitons}}/a \approx 2^{-2/3} \approx 0.63$  for  $J/U = 0.25$ , and  $\ell_{\text{excitons}}/a \approx 5^{1/3}/2 \approx 0.86$  for  $J/U = 0.10$ , showing that the bound state is essentially local with almost no spatial fluctuations. A more detailed analysis beyond the semiclassical approximation made here will be done in an upcoming work.

The physics of the photogeneration of excitons somehow resembles the situation in a slightly doped two-dimensional AFM. There, the holon is trapped in a linear potential created by the AFM background [38]. The excitons reported here can also be related to the dynamics

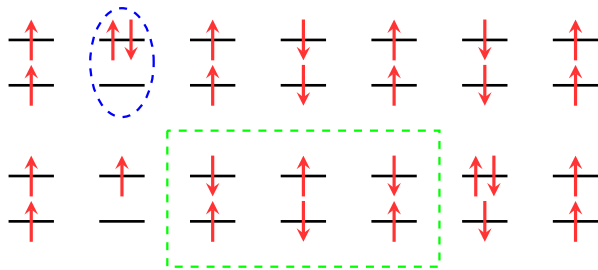


FIG. 5. Cartoon illustrating the stability of Hund excitons in a one-dimensional two-orbital model at half-filling in the Ising limit (ignoring spin fluctuations). The AFM background induces the linear confining potential (14). Starting with a single exciton (top) and subsequently moving the doublon (or analogously the holon) will distort both the local magnetic moment and the AFM background by destroying local triplet states and reducing super-exchange (bottom, dashed box). The magnetic energy loss, which is proportional to the length of the box or number of hops, will generate the trapping potential (14) for the doublon (or analogously, for the holon).

of excitations in spin ladders with AFM intra-chain and FM rung exchanges. There, a singlet propagates in a liquid of triplet states due to a confining potential that hinders strings of misaligned spins. Similar confinement features between holes owed to an interplay of superexchange and delocalization were explored in a two-band Hubbard Hamiltonian [39]. In the two-orbital case considered here, the holon couples locally to the doublon (both having different orbital character) in order to minimize  $V_{\text{excitons}}(x)$  so that the AFM background established by Hund's coupling and superexchange is minimally disturbed, see Fig. 5.

The effect of confinement, or binding, of two fractional excitations has been observed experimentally in the spin systems  $\text{XCo}_2\text{V}_2\text{O}_8$  ( $X = \text{Ba}, \text{Sr}$ ) [40–42]. These quantum magnets can be understood as weakly coupled spin chains with finite anisotropy. Using neutron scattering techniques, the dynamics in such systems was interpreted in terms of spinons interacting via a linear potential induced by inter-chain coupling, which forces them to form a bound state, leading to spinon confinement [40–42]. In the case considered in our work, the confinement occurs not in the spin channel between different chains but in the charge channel between different orbitals, leading to the formation of Hund excitons as discussed in the previous paragraphs.

The experimental detection of Hund excitons can be accomplished, for example, in a pump and probe (time-resolved reflectivity) setup, by registering the evolution of the optical conductivity as a function of both energy and delay time. A resulting midgap or midband state, depending on the values of  $U/W_\gamma$  and  $J/U$ , should be detected between an optical band of unbounded doublon-holon pairs and a precursor of the Drude peak at zero frequency. (There might be multiparticle absorption bands at higher energies that are not relevant to the analysis

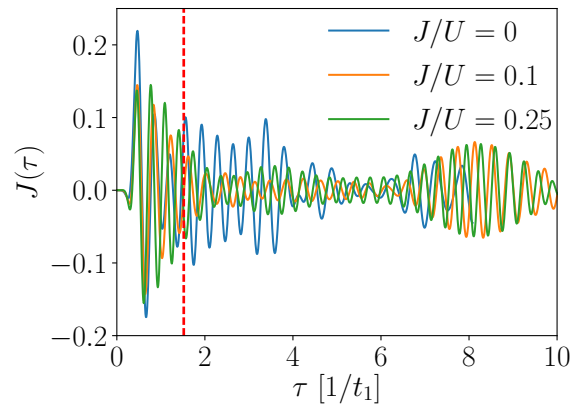


FIG. 6. Electric current density averaged over the system size, for several values of  $J/U$ . The vertical dashed line marks the light pulse span. A long-lived metallic state with a small, albeit finite, oscillating current is found. The photocarriers correspond to a plasma of doublon-holon pairs coexisting with Hund excitons.

here.) Such a midgap/midband peak will correspond to the excitons analyzed here. Material candidates where these excitons could be observed are some perovskite oxides, in particular manganites or nickelates. The relevant physics in those systems should be that of two orbitals.

The corresponding photocurrent resulting from the breakdown of the Mott insulator is displayed in Fig. 6. We observe a transient dynamics, from a high-current state right after the field pulse is applied to a low-current steady state. We note that  $J(\tau)$  displays a similar trend to the intra-orbital correlation  $C_\gamma^{dh}(\tau)$ , indicating a synergy between intra-orbital doublon-holon pairs and photo-carrier dynamics. The oscillations in the current are associated to frequencies related to the inter-orbital repulsion  $U'$  and the charge gap  $\Delta$ . We notice that the revival of the current at later times is due to the system's finite size. The fact that the generation of doublons (see Fig. 1), and therefore Hund excitons, flattens out at late times and the fact that we have a stationary current implies that the excitons coexist with a plasma of mobile carriers (dissociated doublon-holon pairs). In other words, Hund excitons are created up to a saturation point and then the metallic state follows due to their partial dissociation. This in contrast with previous results in single-orbital Hubbard models [21], where a constant creation of doublons has no impact on the current.

As shown by the results on Figs. 1–3, the resulting photoinduced state corresponds to an out-of-equilibrium strongly correlated metal with partially polarized spins and orbital-dependent correlations, with the concurrency of Hund excitons, and doublon-holon plasma as photocarriers. This excitonic metal significantly differs from the equilibrium notion of Hund's metals [37], a metallic state that has been found in the ground state phase diagram of multiorbital Hubbard models [34, 35, 37]. A possible scenario that could be realized at long times is that the current completely decays to zero, leading to the

possibility of a photoinduced phase transition to a Hund-excitonic insulator. A separate future study on the role of fluence and finite size will clarify whether such feature survives in the long-time photoinduced dynamics of the Mott insulator.

It would be interesting to further explore the properties of Hund excitons. Indeed for large values of photodoping, interactions are expected to play a role leading to exciton related phenomena such as formation of biexcitons, crystallization, dissociation, etc. Furthermore, adding a nearest-neighbor repulsion term to the two-orbital Hubbard Hamiltonian might lead to an interesting interplay between Mott-Hubbard and Hund excitons, and likely to the emergence of unexpected quasiparticle dynamics. It would also be interesting to explore the different stages in the breakdown of the Mott insulating state and how it depends on the coupling between radiation and matter. In particular, a study on the intra-band relaxation dynamics in the two-band Mott insulator showed the generation of several excitations [43], among them Hund excitons. We note, however, that the coupling to radiation used in that study differs from the one implemented in our calculations. We are currently investigating the effects of such interactions and couplings to radiation on the dynamics of Hund excitons.

#### IV. CONCLUSIONS

In this work we have studied the photoinduced melting of a two-orbital Mott insulator, resulting in a long-lived nonequilibrium metallic state with unexpected properties. We have also found that the breakdown of the Mott insulating ground state and corresponding onset of the photometallic state, understood as the photogeneration of doublon and holon pairs, is enhanced by the presence of Hund's coupling. Indeed, Hund's coupling tends to suppress doubly-occupied configurations in the ground state, as opposed to the nonequilibrium situation where it greatly enhances doublon production upon interaction with light. The breakdown of the insulating ground state is realized through an insulator to metal photoinduced phase transition with a concomitant melting of the magnetic moment, implying a high- to low-spin light-induced phase transition as well.

Additionally, we have shown evidence that Hund's

coupling *dynamically* activates large orbital fluctuations leading to a nontrivial dynamics of doublon-holon pairs and to the aforementioned light-assisted loss of local magnetic moment and antiferromagnetic quasi-long-range order.

More importantly, we observed the dynamical formation of an emergent neutral and bound quasiparticle with orbital and spin character that is stabilized by Hund's exchange interaction. Such a quasiparticle corresponds to an exciton, which can establish a condensate. In high contrast to the more familiar types of excitonic optical excitations, the exciton studied here is not originated due to direct Coulomb repulsion but due to exchange interactions; in this case Hund's rule coupling. Moreover, we have studied properties of these Hund-exchange-induced excitons such as bandwidth, binding due to a confining potential, and size as a function of Hund's coupling. All these properties can be understood using a semiclassical model that describes the dynamics of bound doublon and holon pairs.

We have also observed that the resulting long-lived photometallic state results as a coexistence of Hund excitons and doublon-holon plasma. This metallic state differs greatly from the more familiar equilibrium idea in multiorbital systems of Hund's metal

#### ACKNOWLEDGMENTS

J.R. acknowledges fruitful conversations with G. Baskaran and Y. Wan and support by the Simons Foundation (Many Electron Collaboration). A.E.F. acknowledges the U.S. Department of Energy, Office of Basic Energy Sciences, for support under grant DE-SC0014407. E.D. was supported by the National Science Foundation under grant No. DMR-1404375. Numerical simulations were performed at the Center for Nanophase Materials Sciences, which is a DOE Office of Science User Facility. This research was supported in part by Perimeter Institute for Theoretical Physics. Research at Perimeter Institute is supported by the Government of Canada through the Department of Innovation, Science and Economic Development Canada and by the Province of Ontario through the Ministry of Research, Innovation and Science.

---

[1] J. Orenstein, *Physics Today* **65**, 44 (2012).

[2] T. Kampftrath, K. Tanaka, and K. A. Nelson, *Nat. Photon.* **7**, 680 (2013).

[3] D. Fausti, R. I. Tobey, N. Dean, S. Kaiser, A. Dienst, M. C. Hoffmann, S. Pyon, T. Takayama, H. Takagi, and A. Cavalleri, *Science* **331**, 189 (2011).

[4] K. Miyano, T. Tanaka, Y. Tomioka, and Y. Tokura, *Phys. Rev. Lett.* **78**, 4257 (1997).

[5] S. Wall, D. Brida, S. R. Clark, H. P. Ehrke, D. Jaksch,

A. Ardavan, S. Bonora, H. Uemura, Y. Takahashi, T. Hasegawa, H. Okamoto, G. Cerullo, and A. Cavalleri, *Nat. Phys.* **7**, 114 (2011).

[6] A. Schiffrin, T. Paasch-Colberg, N. Karpowicz, V. Apalkov, D. Gerster, S. Muhlbrandt, M. Korbman, J. Reichert, M. Schultze, S. Holzner, J. V. Barth, R. Kienberger, R. Ernstorfer, V. S. Yakovlev, M. I. Stockman, and F. Krausz, *Nature* **493**, 70 (2013).

[7] M. Schultze, E. M. Bothschafter, A. Sommer, S. Holzner,

- W. Schweinberger, M. Fiess, M. Hofstetter, R. Kienberger, V. Apalkov, V. S. Yakovlev, M. I. Stockman, and F. Krausz, *Nature* **493**, 75 (2013).
- [8] H. Okamoto, H. Matsuzaki, T. Wakabayashi, Y. Takahashi, and T. Hasegawa, *Phys. Rev. Lett.* **98**, 037401 (2007).
- [9] D. Polli, M. Rini, S. Wall, R. W. Schoenlein, Y. Tomioka, Y. Tokura, G. Cerullo, and A. Cavalleri, *Nat. Mater.* **6**, 643 (2007).
- [10] H. Ehrke, R. I. Tobey, S. Wall, S. A. Cavill, M. Först, V. Khanna, T. Garl, N. Stojanovic, D. Prabhakaran, A. T. Boothroyd, M. Gensch, A. Mirone, P. Reutler, A. Revcolevschi, S. S. Dhesi, and A. Cavalleri, *Phys. Rev. Lett.* **106**, 217401 (2011).
- [11] J. Zhang, X. Tan, M. Liu, S. W. Teitelbaum, K. W. Post, F. Jin, K. A. Nelson, D. N. Basov, W. Wu, and R. D. Averitt, *Nat. Mater.* **15**, 956 (2016).
- [12] B. Casals, R. Cicheler, P. García Fernández, J. Junquera, D. Pesquera, M. Campoy-Quiles, I. C. Infante, F. Sánchez, J. Fontcuberta, and G. Herranz, *Phys. Rev. Lett.* **117**, 026401 (2016).
- [13] M. Fox, *Optical Properties of Solids (Oxford Master Series in Condensed Matter Physics)*, 2nd ed. (Oxford University Press, USA, 2010).
- [14] F. Wooten, *Optical properties of solids* (Academic press, 2013).
- [15] M. Mitrano, G. Cotugno, S. R. Clark, R. Singla, S. Kaiser, J. Stähler, R. Beyer, M. Dressel, L. Baldassarre, D. Nicoletti, A. Perucchi, T. Hasegawa, H. Okamoto, D. Jaksch, and A. Cavalleri, *Phys. Rev. Lett.* **112**, 117801 (2014).
- [16] T. Oka, R. Arita, and H. Aoki, *Phys. Rev. Lett.* **91**, 066406 (2003).
- [17] T. Oka, *Phys. Rev. B* **86**, 075148 (2012).
- [18] K. A. Al-Hassanieh, F. A. Reboledo, A. E. Feiguin, I. González, and E. Dagotto, *Phys. Rev. Lett.* **100**, 166403 (2008).
- [19] F. Heidrich-Meisner, I. González, K. A. Al-Hassanieh, A. E. Feiguin, M. J. Rozenberg, and E. Dagotto, *Phys. Rev. B* **82**, 205110 (2010).
- [20] F. Hofmann and M. Potthoff, *Phys. Rev. B* **85**, 205127 (2012).
- [21] M. Eckstein, T. Oka, and P. Werner, *Phys. Rev. Lett.* **105**, 146404 (2010).
- [22] M. Eckstein and P. Werner, *Phys. Rev. Lett.* **110**, 126401 (2013).
- [23] Y. Kanamori, H. Matsueda, and S. Ishihara, *Phys. Rev. Lett.* **103**, 267401 (2009).
- [24] N. Maeshima, K. Hino, and K. Yonemitsu, *Phys. Rev. B* **82**, 161105 (2010).
- [25] Y. Kanamori, H. Matsueda, and S. Ishihara, *Phys. Rev. Lett.* **107**, 167403 (2011).
- [26] Y. Kanamori, J. Ohara, and S. Ishihara, *Phys. Rev. B* **86**, 045137 (2012).
- [27] S. Ishihara, J. Ohara, and Y. Kanamori, *Eur. Phys. J. Spec. Top.* **222**, 1125 (2013).
- [28] S. R. White, *Phys. Rev. Lett.* **69**, 2863 (1992); *Phys. Rev. B* **48**, 10345 (1993).
- [29] U. Schollwöck, *Rev. Mod. Phys.* **77**, 259 (2005); K. A. Hallberg, *Adv. Phys.* **55**, 477 (2006).
- [30] S. R. White and A. E. Feiguin, *Phys. Rev. Lett.* **93**, 076401 (2004).
- [31] A. J. Daley, C. Kollath, U. Schollwöck, and G. Vidal, *J. Stat. Mech.: Theo. Exp.* **2004**, P04005 (2004).
- [32] A. E. Feiguin and S. R. White, *Phys. Rev. B* **72**, 020404 (2005).
- [33] P. Schmitteckert, *Phys. Rev. B* **70**, 121302 (2004).
- [34] J. Rincón, A. Moreo, G. Alvarez, and E. Dagotto, *Phys. Rev. Lett.* **112**, 106405 (2014).
- [35] J. Rincón, A. Moreo, G. Alvarez, and E. Dagotto, *Phys. Rev. B* **90**, 241105 (2014).
- [36] P. Dai, J. Hu, and E. Dagotto, *Nat. Phys.* **8**, 709 (2012).
- [37] A. Georges, L. de' Medici, and J. Mravlje, *Annu. Rev. Condens. Matter Phys.* **4**, 137 (2013).
- [38] E. Dagotto, *Rev. Mod. Phys.* **66**, 763 (1994).
- [39] K. A. Al-Hassanieh, C. D. Batista, P. Sengupta, and A. E. Feiguin, *Phys. Rev. B* **80**, 115116 (2009).
- [40] B. Grenier, S. Petit, V. Simonet, E. Canévet, L.-P. Regnault, S. Raymond, B. Canals, C. Berthier, and P. Lejay, *Phys. Rev. Lett.* **114**, 017201 (2015).
- [41] A. K. Bera, B. Lake, F. H. L. Essler, L. Vanderstraeten, C. Hubig, U. Schollwöck, A. T. M. N. Islam, A. Schneidewind, and D. L. Quintero-Castro, *arXiv:1705.01259* (2017).
- [42] Q. Faure, S. Takayoshi, S. Petit, V. Simonet, S. Raymond, L.-P. Regnault, M. Boehm, J. White, M. Månsson, C. Rüegg, P. Lejay, B. Canals, S. Furuya, T. Giamarchi, and B. Grenier, *arXiv:1706.05848* (2017).
- [43] H. U. R. Strand, D. Golež, M. Eckstein, and P. Werner, *arXiv:1704.06101* (2017).